Communications on Applied Mathematics and Computation
https://doi.org/10.1007/s42967-024-00470-2

ORIGINAL PAPER

A Hybrid HWENO Scheme for a Multi-class Traffic Flow Model with Heterogeneous Factors on Highroad

Qi Meng[1] · **Jianxian Qiu**[1]

Received: 20 July 2024 / Revised: 18 October 2024 / Accepted: 30 November 2024

Abstract
A hybrid fifth-order finite volume Hermite weighted essentially non-oscillatory (HWENO) scheme is applied for the solution of a multi-class traffic flow model (mcLWR model) with heterogeneous factors on the highroad. Since the hybrid HWENO scheme could avoid oscillations near discontinuities while maintaining efficiency and compactness, it can be a reliable numerical method and tool for the simulation and prediction of rapidly changing the traffic flow. The benchmark examples of Riemann problems and traffic signal control problems are given, and results indicate that the hybrid HWENO numerical scheme can obtain the fifth-order precision, and also has higher resolution and accuracy than the hybrid WENO scheme.

Keywords Hermite weighted essentially non-oscillatory (HWENO) scheme · Multi-class traffic flow model (mcLWR model) · Non-strictly hyperbolicity · Discontinuous flux · Heterogeneous factors on highway

Mathematics Subject Classification 35L65 · 65M60

1 Introduction

A fundamental traffic flow model (LWR model) is proposed to describe traffic flow characteristics, it is a simplified continuum model given by Lighthill and Whitham [13], and Richards [20] independently. This model supplements the relationship between traffic variables such as traffic density, car stream, and vehicle speed with the vehicle continuity equation. The resultant PDE gives the density as a function of time and space. A specific format for the Greenshields [8] model of vehicle flow can get the analytic solution [27]. Although originally intended for simulating traffic phenomena, LWR models demonstrate the capability to qualitatively replicate various real-world traffic behaviors, including the formation of shocks.

✉ Jianxian Qiu
jxqiu@xmu.edu.cn

Qi Meng
qmeng@stu.xmu.edu.cn

[1] School of Mathematical Sciences and Fujian Provincial Key Laboratory of Mathematical Modeling and High-Performance Scientific Computing, Xiamen University, Xiamen 361005, Fujian, China

However, some perplexing expressway traffic phenomena cannot be explained by simple LWR models, like the two-capacity, queue discreteness, and the lag of vehicle flow.

The above traffic phenomena are then explained by the development of a multi-class model that incorporates the lane changing behavior of users and a variety of vehicle types [5, 6]. Based on the LWR model, Wong and Wong [26] considered different drivers and proposed the mcLWR model. Despite its simplicity, the mcLWR model has demonstrated its ability to generate the necessary properties for macroscopic traffic flow models. Along with the heterogeneous traffic flow problem has been the focus of research, Zhang et al. [30] extended the mcLWR model to deal with heterogeneous road factors. This extension holds significant practical applications and theoretical implications. In real-world traffic scenarios, variations in traffic capacity frequently occur in many places, like near corners, ramps, slopes, and areas prone to car accidents. This expansion effectively incorporates these traffic phenomena into the model.

After extending the mcLWR model, solving the system may become more complex due to the spatial variation in fluxes, particularly because the flux is discontinuous. In [25], Wong and Wong used the first-order Lax-Friedrichs finite difference scheme to get the solution of the mcLWR model, but that method introduces excessive numerical viscosity, resulting in smeared solutions near discontinuities. Subsequently, Lebacque [12] successfully used the Godunov scheme [7] to deal with the LWR traffic flow model. While this approach demonstrates a reduction in numerical viscosity, it relies on the Riemann solver as its fundamental component which can be challenging for mcLWR models and may not be feasible. References [30] and [22] employed the WENO scheme and DG scheme to handle the mcLWR model, respectively, and proved that both schemes are more effective than Lax-Friedrichs schemes and Godunov numerical schemes.

In this article, we use a hybrid fifth-order HWENO scheme to solve the mcLWR model with heterogeneous factors on the highway. The HWENO scheme is an evolution of the ENO and WENO schemes, both of them have been extensively used for hyperbolic conservation laws for the past few years. Qiu and Shu [17, 18] pioneered the WENO methodology, initially applying it as limiters for Runge-Kutta discontinuous Galerkin methods, leading to the development of HWENO schemes. Subsequently, various HWENO schemes [3, 4, 15, 16, 23, 24, 33] have been created to address hyperbolic conservation laws. The hybrid HWENO scheme in this text combines the discontinuous Galerkin method limiter to control oscillations, thus it is superior to the previous HWENO scheme [17, 18], see [31] for details.

The rest is structured as follows. The conservation form for the mcLWR model equation is briefly provided in Sect. 2. Section 3 presents a discussion on a hybrid HWENO scheme applied to a modified equivalent system, utilizing the Lax-Friedrichs numerical flux within the finite volume method. Section 4 showcases numerical tests to validate the proposed scheme's accuracy, efficiency, and robustness. Finally, Sect. 5 offers concluding remarks.

2 Description of Conservation Form for the mcLWR Model with Inhomogeneous Factors

In traffic flow, the vehicles' types are m and vehicles' lanes are $l(x)$. The density of each lane of type i vehicles is $\rho_i(x,t)$, and the density of each vehicles type is given by

$$u_i(x,t) = l(x)\rho_i(x,t),$$

and $\rho = \sum_{i=1}^{m} \rho_i$ represents the total density of each lane. The vehicle speed depends on the density, denoted by $v(\rho)$, with $v(0) = v_{\mathrm{f}}$ when the density is zero (free-flow speed) and $v(\rho_{\mathrm{jam}}) = 0$ at the jam density, decreasing with increasing the density $v'(\rho) < 0$. In calculation, $v(\rho) = (\rho_{\mathrm{jam}} - \rho)v_{\mathrm{f}}/\rho_{\mathrm{jam}}$, that is, the velocity has a linear relationship with the density [8, 27]. The difference between vehicle types, represented by the dimensionless variable $\{d_i(x)\}_{i=1}^{m}$, where $0 \leqslant d_i(x) \leqslant 1$ for all i. The speed of vehicle type i is then $v_i(x,t) = d_i(x)v(\rho)$.

From the mass conservation of m vehicle types on the road, we can get the system equations

$$(l(x)\rho_i(x,t))_t + (l(x)\rho_i(x,t)d_i(x)v(\rho(x,t)))_x = 0, \quad 1 \leqslant i \leqslant m. \tag{1}$$

Let the vector function $\theta(x) = (l(x), d_1(x), \cdots, d_m(x))$ represent the improved or reduced traffic capacity at the corresponding position. Because the degree of change is very dramatic, θ can be considered as a discontinuous function of x during its changes, resulting in the discontinuity of the flux function as well. Given that the spatial variation of the flux can lead to the discontinuity of the flux, directly applying standard numerical methods to the system may be inefficient. Therefore, utilizing the construction with an equivalent form [2] of the conservation law for handling spatially varying fluxes [1, 10, 14, 28], the system equations could be written as the $(m+1) \times (m+1)$ format [30]:

$$\frac{\partial}{\partial t}\begin{pmatrix} l\rho_1 \\ l\rho_2 \\ \vdots \\ l\rho_m \\ \theta \end{pmatrix} + \frac{\partial}{\partial x}\begin{pmatrix} l\rho_1 d_1 v(\rho) \\ l\rho_2 d_2 v(\rho) \\ \vdots \\ l\rho_m d_m v(\rho) \\ 0 \end{pmatrix} = 0. \tag{2}$$

For convenience, in applying numerical schemes in the next section, we denote $\boldsymbol{U} = (l\rho_1, l\rho_2, \cdots, l\rho_m, \theta)^{\mathrm{T}}$, $\boldsymbol{F} = (l\rho_1 d_1 v, l\rho_2 d_2 v, \cdots, l\rho_m d_m v, 0)^{\mathrm{T}}$. Equation (2) can be abbreviated as

$$\boldsymbol{U}_t + \boldsymbol{F}_x = 0.$$

Remark 1 For the mcLWR model with inhomogeneous factors, Zhang et al. studied the hyperbolicity and characteristic fields of the system, see [30] in detail. The Jacobian matrix $\boldsymbol{F}'(\boldsymbol{U})$ that will be used for a characteristic decomposition in latter numerical experiments can also be found in [30].

Remark 2 For the Riemann problem of (1), the propagation properties of shock waves and rarefaction waves have been studied in [29], and we will not repeat it here.

3 Description of the Hybrid HWENO Scheme

The hybrid HWENO scheme was developed to solve hyperbolic conservation laws in [31]. We now present the scheme for the mcLWR equations with inhomogeneous conditions

$$\frac{\partial \boldsymbol{U}}{\partial t} + \frac{\partial \boldsymbol{F}(\boldsymbol{U})}{\partial x} = 0, \tag{3}$$

where

$$\boldsymbol{U} = \begin{pmatrix} u \\ \theta \end{pmatrix}, \boldsymbol{F} = \begin{pmatrix} f \\ o \end{pmatrix},$$

and the flux $o = 0$. The calculation interval is divided into N equal parts that are denoted as $\{x_{1/2}, x_{3/2}, \cdots, x_{N+1/2}\}$. Interval I_k is $[x_{k-1/2}, x_{k+1/2}]$, h denotes the grid size, the cell center point is $x_k = 0.5(x_{k-1/2} + x_{k+1/2})$, and $x_{k+j} = x_k + jh$.

The semi-discrete finite volume HWENO scheme of (3) is given by

$$\begin{cases} \dfrac{\mathrm{d}\overline{\boldsymbol{U}}_k(t)}{\mathrm{d}t} = -\left(\hat{\boldsymbol{F}}_{k+1/2} - \hat{\boldsymbol{F}}_{k-1/2}\right)/h, \\ \dfrac{\mathrm{d}\widetilde{\boldsymbol{U}}_k(t)}{\mathrm{d}t} = \left(-\left(\hat{\boldsymbol{F}}_{k-1/2} + \hat{\boldsymbol{F}}_{k+1/2}\right) + 2\boldsymbol{T}_k\right)/(2h), \end{cases} \tag{4}$$

where the cell average $\overline{\boldsymbol{U}}_k(t)$ is $\frac{1}{h}\int_{I_k} \boldsymbol{U}(x,t)\mathrm{d}x$ and the first order moment $\widetilde{\boldsymbol{U}}_k(t)$ is defined as $\frac{1}{h}\int_{I_k} \boldsymbol{U}(x,t)\frac{x-x_k}{h}\mathrm{d}x$. We apply the Lax-Friedrichs numerical flux as follows:

$$\hat{\boldsymbol{F}}_{k-1/2} = \frac{1}{2}\left(\boldsymbol{F}(\boldsymbol{U}^-_{k-1/2}) + \boldsymbol{F}(\boldsymbol{U}^+_{k-1/2}) - \alpha\left(\boldsymbol{U}^+_{k-1/2} - \boldsymbol{U}^-_{k-1/2}\right)\right),$$

where $\alpha = \max_{\boldsymbol{U}} |\boldsymbol{F}'(\boldsymbol{U})|$. $\boldsymbol{T}_k$ is the numerical integration of the flux $\boldsymbol{F}(\boldsymbol{U})$, which is approximated by the four-point Gauss-Lobatto quadrature formula. The weights and the quadrature points on I_k are $\{w_l^{\mathrm{G}}\}_{l=1}^4 = \{\frac{1}{12}, \frac{5}{12}, \frac{5}{12}, \frac{1}{12}\}$ and $\{x_l^{\mathrm{G}}\}_{l=1}^4 = \{x_{k-\frac{1}{2}}, x_{k-\frac{\sqrt{5}}{10}}, x_{k+\frac{\sqrt{5}}{10}}, x_{k+\frac{1}{2}}\}$, and

$$\boldsymbol{T}_k = \frac{1}{h}\int_{I_k} \boldsymbol{F}(\boldsymbol{U})\mathrm{d}x \approx \sum_{l=1}^{4} \omega_l^{\mathrm{G}} \boldsymbol{F}(\boldsymbol{U}(x_l^{\mathrm{G}}, t)).$$

Now, we show the details of the spatial reconstruction. Orthogonal basis functions $\{G_i(x), i = 0, \cdots, r\}$ are used in calculations, in I_k Legendre polynomials are adopted:

$$\left\{G_0(x) = 1, G_1(x) = \xi_k, G_2(x) = \xi_k^2 - \frac{1}{12}, G_3(x) = \xi_k^3 - \frac{3}{20}\xi_k, \cdots\right\},$$

where $\xi_k = \frac{x-x_k}{h}$, and $\overline{U}_k$ is the cell average, and $\widetilde{U}_k$ is the first order moment of solution in cell I_k in actual calculation.

i) Inspect which I_k is discontinuous and limit $\widetilde{U}$ in I_k.

First of all, we need to identify the troubled-cell in which the solution is broken. There are many troubled-cell indicators in the literature which can be adopted, following the suggestion by Qiu and Shu in [19], we use the KXRCF indicator [11] to find the discontinuities in this paper. Because traffic flows from left to right, the cell I_k will be recognized as a troubled cell, if

$$\frac{\left| U^h_{I_k}(x_{k-1/2}) - U^h_{I_{k-1}}(x_{k-1/2}) \right|}{\max_{x\in I_k} |U^h_{I_k}(x)|\, c^{\frac{r+1}{2}}} > 1,$$

where $c = h/2$. We use second-order polynomials U_h to approximate $U(x)$, so $r = 2$ in this problem. $\overline{U}_{k-1}$, $\overline{U}_k$, $\overline{U}_{k+1}$, and $\widetilde{U}_k$ are used to reconstruct a cubic polynomial $P_k^3(x) = \sum_{j=0}^3 b_j G_j(x)$ which satisfies

$$\frac{1}{h}\int_{I_{k+i}} P_k^3(x)\mathrm{d}x = \overline{U}_{k+i}, \quad i = -1, 0, 1, \quad \frac{1}{h}\int_{I_k} P_k^3(x)\xi_k\mathrm{d}x = \widetilde{U}_k.$$

And then project $P_k^3(x)$ onto the quadratic space of the quadratic orthogonal function space, $U^h_{I_k}$ is taken as $\overline{U}_k G_0(x) + 12\widetilde{U}_k G_1(x) + \frac{1}{2}(\overline{U}_{k+1} - 2\overline{U}_k + \overline{U}_{k-1})G_2(x)$. The polynomial is

used only in the troubled-cell indicator to identify the troubled cell, not in the reconstruction procedure for solution, so drop the cubic term will not affect accuracy.

After identifying troubled cells, the first moment of the troubled cells is modified by using the HWENO limiter given in [31] and the counterpart of other cells remains unchanged.

ii) The calculation procedure of Gauss-Lobatto integration points.

Let $L_{\mathrm{U}}(\cdot)$, $L_{\mathrm{V}}(\cdot)$ represent the right-hand sides of (4), respectively. To calculate these two terms, we need the solution values at $x_{k\pm 1/2}$ and $x_{k\pm\sqrt{5}/10}$ in all cells. The HWENO reconstruction is applied to solve the boundary points $U^{\mp}_{k\pm 1/2}$ in troubled cells, and the linear approximation is adopted to solve the integral points $U_{k\pm\sqrt{5}/10}$ in all cells and the boundary points in the smooth cells.

(i) The procedure to reconstruct $U^{-}_{k+1/2}$ by the HWENO.

The HWENO reconstruction uses three cubic polynomials $P_j^3(x) = \sum_{l=0}^{3} a_l^j G_l(x)$, where $j = 1, 2, 3$ to create a quintic polynomial $P_0^5(x) = \sum_{l=0}^{5} a_l G_l(x)$, the three cubic polynomials are obtained by

$$\begin{aligned}
&\frac{1}{h}\int_{I_{k+i}} P_1^3(x)\mathrm{d}x = \overline{U}_{k+i}, \quad \frac{1}{h}\int_{I_{k+i}} P_1^3(x)\xi_{k+i}\mathrm{d}x = \widetilde{U}_{k+i}, \quad i = -1, 0,\\
&\frac{1}{h}\int_{I_{k+i}} P_2^3(x)\mathrm{d}x = \overline{U}_{k+i}, \quad i = -1, 0, 1, \quad \frac{1}{h}\int_{I_k} P_2^3(x)\xi_k\mathrm{d}x = \widetilde{U}_k,\\
&\frac{1}{h}\int_{I_{k+i}} P_3^3(x)\mathrm{d}x = \overline{U}_{k+i}, \quad \frac{1}{h}\int_{I_{k+i}} P_3^3(x)\xi_{k+i}\mathrm{d}x = \widetilde{U}_{k+i}, \quad i = 0, 1,
\end{aligned}$$

the explicit expressions of $\{a_l^j\}$ are

$$\begin{cases}
a_0^1 = \overline{U}_k,\\
a_1^1 = 12\widetilde{U}_k,\\
a_2^1 = (114\widetilde{U}_k + 66\widetilde{U}_{k-1} - 15\overline{U}_k + 15\overline{U}_{k-1})/4,\\
a_3^1 = (30\widetilde{U}_k + 30\widetilde{U}_{k-1} - 5\overline{U}_k + 5\overline{U}_{k-1})/2,
\end{cases}
\begin{cases}
a_0^2 = \overline{U}_k,\\
a_1^2 = 12\widetilde{U}_k,\\
a_2^2 = (\overline{U}_{k+1} - 2\overline{U}_k + \overline{U}_{k-1})/2,\\
a_3^2 = (-120\widetilde{U}_k + 5\overline{U}_{k+1} - 5\overline{U}_{k-1})/11,
\end{cases}$$

$$\begin{cases}
a_0^3 = \overline{U}_k,\\
a_1^3 = 12\widetilde{U}_k,\\
a_2^3 = (-66\widetilde{U}_{k+1} - 114\widetilde{U}_k + 15\overline{U}_{k+1} - 15\overline{U}_k)/4,\\
a_3^3 = (30\widetilde{U}_{k+1} + 30\widetilde{U}_k - 5\overline{U}_{k+1} + 5\overline{U}_k)/2,
\end{cases}$$

the quintic polynomials $P_0(x)$ are obtained by

$$\frac{1}{h}\int_{I_{k+i}} P_0^5(x)\mathrm{d}x = \overline{U}_{i+k}, i = -1, 0, 1, \quad \frac{1}{h}\int_{I_{k+i}} P_0^5(x)\xi_{k+i}\mathrm{d}x = \widetilde{U}_{k+i}, i = -1, 0, 1,$$

and the explicit expressions of $\{a_l\}$ are

$$\begin{cases}
a_0 = \overline{U}_k,\\
a_1 = 12\widetilde{U}_k,\\
a_2 = (-270\widetilde{U}_{k+1} + 270\widetilde{U}_{k-1} + 73\overline{U}_{k+1} - 73\overline{U}_k + 73\overline{U}_{k-1})/56,\\
a_3 = (-1\,970\widetilde{U}_{k+1} - 10\,340\widetilde{U}_k - 1\,970\widetilde{U}_{k-1} + 595\overline{U}_{k+1} - 595\overline{U}_{k-1})/324,\\
a_4 = (30\widetilde{U}_{k+1} - 30\widetilde{U}_{k-1} - 5\overline{U}_{k+1} + 10\overline{U}_k - 5\overline{U}_{k-1})/8,\\
a_5 = (154\widetilde{U}_{k+1} + 532\widetilde{U}_k + 154\widetilde{U}_{k-1} - 35\overline{U}_{k+1} + 35\overline{U}_{k-1})/36.
\end{cases}$$

The linear weights $R_1 = \frac{14}{27}$, $R_2 = \frac{22}{63}$, and $R_3 = \frac{25}{189}$ are obtained from the following formula:

$$P_0^5(x_{k-1/2}) = \sum_{l=1}^{3} R_l P_l^5(x_{k-1/2}),$$

then, the smoothness indicators β_l [31] in I_k are computed to detect the smoothness of the function $P_l(x)$,

$$\beta_l = \sum_{\gamma=1}^{r} \int_{I_k} h^{2\gamma-1} \Big(\frac{\mathrm{d}^\gamma P_l(x)}{\mathrm{d}x^\gamma} \Big)^2 \mathrm{d}x, \quad l = 1, 2, 3,$$

where r is the degree of $P_l(x)$, and β_l $(l = 1, 2, 3)$ are as follows:

$$\begin{cases} \beta_1 = \frac{1}{16}(54\widetilde{U}_k + 6\widetilde{U}_{k-1} - \overline{U}_k + \overline{U}_{k-1})^2 + \frac{13}{48}(114\widetilde{U}_k + 66\widetilde{U}_{k-1} - 15\overline{U}_k + 15\overline{U}_{k-1})^2 \\ \qquad + \frac{3\,905}{16}(6\widetilde{U}_k + 6\widetilde{U}_{k-1} - \overline{U}_k + \overline{U}_{k-1})^2, \\ \beta_2 = \frac{1}{484}(-240\widetilde{U}_k - \overline{U}_{k+1} + \overline{U}_{k-1})^2 + \frac{13}{12}(\overline{U}_{k+1} - 2\overline{U}_k + \overline{U}_{k-1})^2 \\ \qquad + \frac{355}{44}(24\widetilde{U}_k - \overline{U}_{k+1} + \overline{U}_{k-1})^2, \\ \beta_3 = \frac{1}{16}(6\widetilde{U}_{k+1} + 54\widetilde{U}_k - \overline{U}_{k+1} + \overline{U}_k)^2 + \frac{13}{48}(66\widetilde{U}_{k+1} + 114\widetilde{U}_k - 15\overline{U}_{k+1} + 15\overline{U}_k)^2 \\ \qquad + \frac{3\,905}{16}(6\widetilde{U}_{k+1} + 6\widetilde{U}_k - \overline{U}_{k+1} + \overline{U}_k)^2. \end{cases}$$

Therefore, the value of $U_{k-1/2}^+$ is

$$U_{k-1/2}^+ = \sum_{l=1}^{3} W_l P_l(x_{k-1/2}),$$

the nonlinear weights $W_l = \overline{W}_l/(\overline{W}_1 + \overline{W}_2 + \overline{W}_3)$, with $\overline{W}_l = R_l/(\beta_l + \varepsilon)^2$, $l = 1, 2, 3$, and $\varepsilon = 10^{-6}$ is adopted to avoid the denominator by zero. $U_{k+1/2}^-$ can be obtained in the above step with respect to the mirror symmetry of x_k.

(ii) Reconstruction to get $U_{k\pm1/2}^{\mp}$ by the linear approximation.

If I_k is a smooth unit, we just use $P_0^5(x)$ in Step (i) to approximate $U_{k\pm1/2}^{\mp}$, namely

$$U_{k-1/2}^+ = P_0^5(x_{k-1/2}) = -\frac{25}{54}\widetilde{U}_{k+1} - \frac{241}{54}\widetilde{U}_k + \frac{28}{27}\widetilde{U}_{k-1} + \frac{13}{108}\overline{U}_{k+1} + \frac{7}{12}\overline{U}_k + \frac{8}{27}\overline{U}_{k-1},$$

and

$$U_{k+1/2}^- = P_0^5(x_{k+1/2}) = -\frac{28}{27}\widetilde{U}_{k+1} + \frac{241}{54}\widetilde{U}_k + \frac{25}{54}\widetilde{U}_{k-1} + \frac{8}{27}\overline{U}_{k+1} + \frac{7}{12}\overline{U}_k + \frac{13}{108}\overline{U}_{k-1}.$$

(iii) The linear approximation to get $U_{k\pm\sqrt{5}/10}$.

Same as above,

$$\begin{aligned} U_{k-\sqrt{5}/10} = P_0^5(x_{k-\sqrt{5}/10}) = &\Big(\frac{3}{20} - \frac{841}{13\,500}\sqrt{5}\Big)\widetilde{U}_{k+1} - \frac{10\,289}{6\,750}\sqrt{5}\widetilde{U}_k - \Big(\frac{3}{20} + \frac{841}{13\,500}\sqrt{5}\Big)\widetilde{U}_{k-1} \\ &+ \Big(\frac{101}{5\,400}\sqrt{5} - \frac{1}{24}\Big)\overline{U}_{k+1} + \frac{13}{12}\overline{U}_k - \Big(\frac{101}{5\,400}\sqrt{5} + \frac{1}{24}\Big)\overline{U}_{k-1}, \end{aligned}$$

and

$$U_{k+\sqrt{5}/10} = P_0^5\left(x_{k+\sqrt{5}/10}\right) = \left(\frac{3}{20} + \frac{841}{13\,500}\sqrt{5}\right)\widetilde{U}_{k+1} + \frac{10\,289}{6\,750}\sqrt{5}\widetilde{U}_k + \left(\frac{841}{13\,500}\sqrt{5} - \frac{3}{20}\right)\widetilde{U}_{k-1} - \left(\frac{101}{5\,400}\sqrt{5} + \frac{1}{24}\right)\overline{U}_{k+1} + \frac{13}{12}\overline{U}_k + \left(\frac{101}{5\,400}\sqrt{5} - \frac{1}{24}\right)\overline{U}_{k-1}.$$

iii) After completing the previous steps, let $\boldsymbol{Z} = (\boldsymbol{U}, \boldsymbol{V})^{\mathrm{T}}$, $L(\cdot) = (L_{\mathrm{U}}(\cdot), L_{\mathrm{V}}(\cdot))^{\mathrm{T}}$. The third-order TVD Runge-Kutta method [21] is applied to do the time discretization of the ordinary differential equation (4):

$$\begin{cases} \boldsymbol{Z}^{(1)} = \boldsymbol{Z}^n + \Delta t L(\boldsymbol{Z}^n), \\ \boldsymbol{Z}^{(2)} = \frac{3}{4}\boldsymbol{Z}^n + \frac{1}{4}\boldsymbol{Z}^{(1)} + \frac{1}{4}\Delta t L(\boldsymbol{Z}^{(1)}), \\ \boldsymbol{Z}^{(n+1)} = \frac{1}{3}\boldsymbol{Z}^n + \frac{2}{3}\boldsymbol{Z}^{(2)} + \frac{2}{3}\Delta t L(\boldsymbol{Z}^{(2)}). \end{cases}$$

Remark 3 As stated in Sect. 2, the traffic flow equations will have non-strictly hyperbolic cases, so the HWENO approximation is used with a local characteristic field decomposition when the systems are strictly hyperbolic and it is used component by component when the systems are non-strictly hyperbolic. As for the linear approximation, it is always used component by component.

4 Numerical Tests

In the following, the numerical accuracy of the hybrid HWENO and hybrid WENO schemes [32] is checked first. Subsequently, we present the numerical results for the Riemann problem and the traffic signal control problem solved using both methods. For all numerical experiments in this section, the CFL number = 0.6, except for the traffic signal control examples, where it is set to 0.3. All of the methods used the fifth order.

In all numerical results, ρ_l and ρ are normalized by blocking the density ρ_{jam}, and the computational area $(0, L)$ is scaled to $(0, 1)$. These dimensionless variables are used wherever units are not specified. Additionally, the constants $L = 8\,000$ m and $v_{\mathrm{f}} = 20\,\mathrm{m{\cdot}s^{-1}}$ are consistently applied.

Example 1 (Test of accuracy) To examine the accuracy of these two methods, the smooth initial data we set are as follows:

$$u_1(x, 0) = 0.1\sin(2\pi x) + 0.3,\ u_2(x, 0) = 0.2,$$
$$u_3(x, 0) = -0.1\sin(2\pi x) + 0.4,\ l(x) = 0.1\sin(2\pi x) + 1,$$
$$d_i(x) = b_i(1 + 0.5\sin(2\pi x)),\ i = 1, 2, 3 \text{ with } b_1 = 0.2, b_2 = 0.3, b_3 = 0.4.$$

We apply the periodic boundary conditions in the smooth test, setting the simulation time to $t = 0.1$, which is sufficiently short to maintain a smooth solution and prevent any discontinuities for $t \leqslant 0.1$. Using the third-order TVD Runge-Kutta time discretization, we set $\Delta t^{(n)} = 0.6\Delta x^{5/3}/\alpha^{(n)}$ to achieve the fifth-order accuracy in both schemes (Table 1).

Example 2 (Riemann problem) Consider the Riemannian problem designed to reproduce the analysis of shock and rarefaction waves patterns:

$$u(x, 0) = \begin{cases} u_{\mathrm{left}}, & \text{if } x < x_0, \\ u_{\mathrm{right}}, & \text{if } x > x_0, \end{cases} \quad \theta(x) = \begin{cases} \theta_{\mathrm{left}}, & \text{if } x < x_0, \\ \theta_{\mathrm{right}}, & \text{if } x > x_0. \end{cases}$$

Table 1 Test of accuracy: the hybrid HWENO scheme and the hybrid WENO scheme. L^1, L^∞ errors and orders of $\sum_{k=1}^{3} U_k$

	Hybrid HWENO scheme				Hybrid WENO scheme			
N cells	L^1 error	Order	L^∞error	Order	L^1 error	Order	L^∞ error	Order
20	2.46E−08		4.55E−08		1.40E−06		4.17E−06	
40	7.06E−10	5.12	1.49E−09	4.93	5.08E−08	4.79	1.72E−07	4.60
80	2.17E−11	5.03	4.67E−11	4.99	1.65E−09	4.94	5.74E−09	4.91
160	6.73E−13	5.01	1.46E−12	5.00	5.20E−11	4.99	1.82E−10	4.98
320	2.10E−14	5.00	4.64E−14	4.97	1.63E−12	5.00	5.71E−12	4.99

The number of vehicle types is set to $m = 3$, which is the sufficiently small number where the breaking wave can be observed. For each i, to facilitate solving, $d_i(x)$ are set to constant, namely, $d_1(x) = 0.5$, $d_2(x) = 0.75$, and $d_3(x) = 1$. The simulation time is taken as 400 s. Here, we use two methods to calculate four numerical examples, Figs. 1–4 show the numerical results. The four kinds of initial data that have been scaled are as follows:

$$\text{(a)}\quad (u_1, u_2, u_3, l) = \begin{cases} (0.60, 0.3, 0.9, 3), & x \leqslant 0.5, \\ (0.10, 0, 0.5, 1), & x > 0.5. \end{cases}$$

$$\text{(b)}\quad (u_1, u_2, u_3, l) = \begin{cases} (0.6, 0.15, 0.3, 3), & x \leqslant 0.4, \\ (0.3, 0.25, 0.15, 1), & x > 0.4. \end{cases}$$

$$\text{(c)}\quad (u_1, u_2, u_3, l) = \begin{cases} (0.6, 0.45, 0.15, 3), & x \leqslant 0.3, \\ (0.05, 0.15, 0.2, 1), & x > 0.3. \end{cases}$$

$$\text{(d)}\quad (u_1, u_2, u_3, l) = \begin{cases} (0.9, 0.6, 0.3, 3), & x \leqslant 0.4, \\ (0.15, 0.25, 0.05, 1), & x > 0.4. \end{cases}$$

With the high profile resolution, the wave structure structures in Figs. 1–4 are consistent with the results analyzed in [30]. Actually, we observe four waves in Figs. 1 and 2 and five waves in Figs. 3 and 4. In the former case, the hyperbolic property of this system is strict, with a single wave propagating either in $x > x_0$ (Fig. 1) or $x < x_0$ (Fig. 2). In the latter case, two characteristics propagate in $x < x_0$ and $x > x_0$, respectively, indicating the system's non-strict hyperbolicity.

In summary, we can see that the computed densities ρ_1, ρ_2, ρ_3 by both the hybrid HWENO scheme and hybrid WENO scheme show the good consistency with reference solutions and are in accordance with the conclusions of the previous analysis. Furthermore, it can be seen that the solution by the hybrid HWENO scheme has a better performance. Additionally, the hybrid HWENO scheme demonstrates the superior performance, providing better approximation results and effectively reducing oscillations due to its more compact stencil.

Example 3 (Traffic signal control problem) We apply numerical schemes to applications where θ is also a function of the time, a common scenario in road traffic, with the traffic light control being a classic example. At the beginning, the traffic light signals the vehicle to stop and wait. After waiting for 30 s, the traffic light signals that the vehicle can pass. After another 30 s, the traffic light turns red again. To model this periodic signal change, we consider a road segment of 1 200 m in length with a constant number of lanes ($l(x) = l$). The traffic signal is located at approximately 420 m. The initial conditions for vehicle densities are $(\rho_1, \rho_2, \rho_3)^{\mathrm{T}} = (0.05, 0.25, 0.1)^{\mathrm{T}}$. We assume that when the signal is green, all $\{d_i(x)\}_{i=1}^{3}$

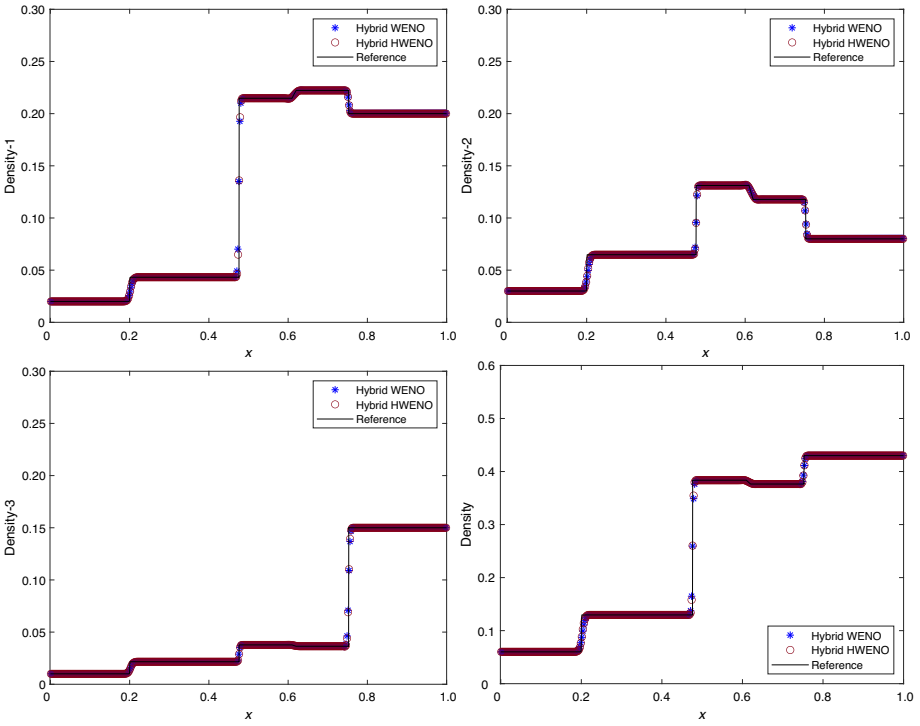

Fig. 1 Example 2. Under the initial condition (a), the hybrid HWENO scheme (red circle) and the hybrid WENO scheme (blue star) with $N = 400$ cells are used to calculate the densities at $t = 1$, and the solution solved by the WENO (solid black line) with $N = 16\,000$ cells is used as a reference. ρ_1, ρ_2, ρ_3, and the total density ρ are plotted in subgraphics

are the same as in the previous example. However, at the signal location and during the red light, all $\{d_i(x)\}_{i=1}^3$ are set to zero, as described below:

$$(d_1, d_2, d_3) = \begin{cases} (0, 0, 0), & \text{if } \ 0.34 < x < 0.36 \ \text{ and } \ 0 < t - 60[t/60] \leqslant 30\,\text{s}, \\ (0.5, 0.75, 1), & \text{otherwise.} \end{cases}$$

Figure 5 presents the numerical results of densities over a 30-second interval. From Fig. 5 a line of the stationary traffic is obviously visible before the traffic light crossing, propagating backward when the green light is on. In the queue of the traffic flow, ρ is at its peak. To the right of the traffic light crossing, three shock waves can be observed, leaving behind a long vacuum representing the overtaking among three different vehicle types. Figure 6 illustrates the total density evolution over a 60-second period, describing overtaking behavior in real traffic flow, a prominent feature of the model discussed. The propagation of three waves in Fig. 6 matches the vehicle types, and shows dissipation and queuing close to the traffic light crossing.

The simulation of the traffic signal control can be conducted for any duration because the signal changes periodically, and the number of vehicles can be arbitrarily large. In theory, the hybrid HWENO scheme should address conservation laws with discontinuous fluxes in various research fields.

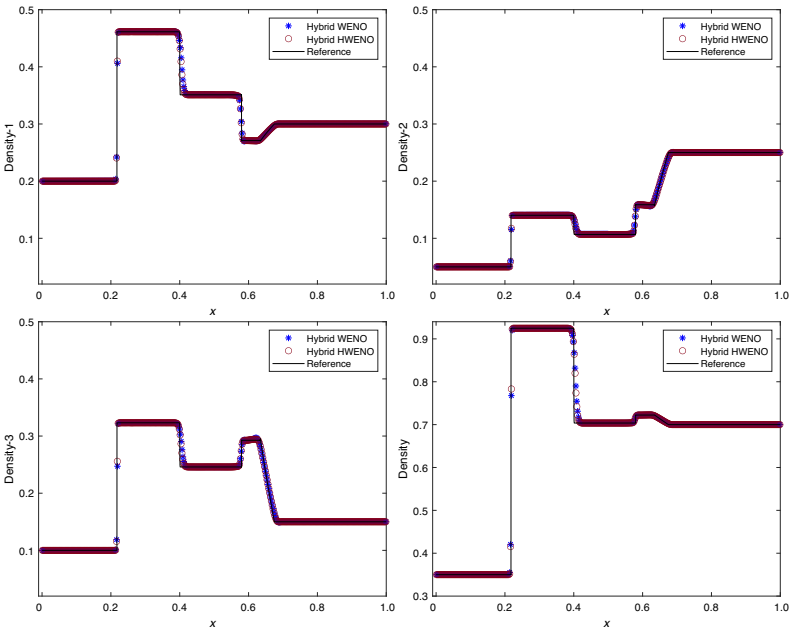

Fig. 2 Same as Fig. 1, except for the initial condition (b)

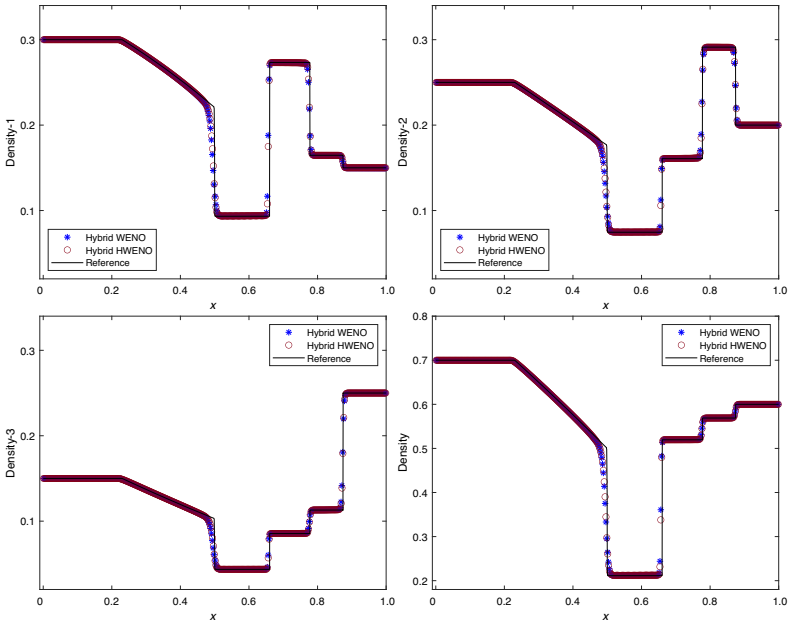

Fig. 3 Same as Fig. 1, except for the initial condition (c)

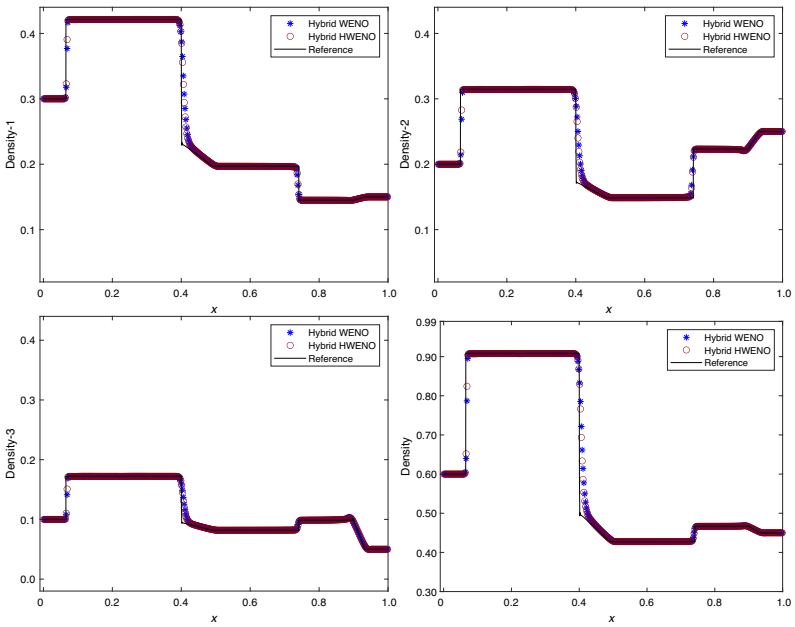

Fig. 4 Same as Fig. 1, except for the initial condition (d)

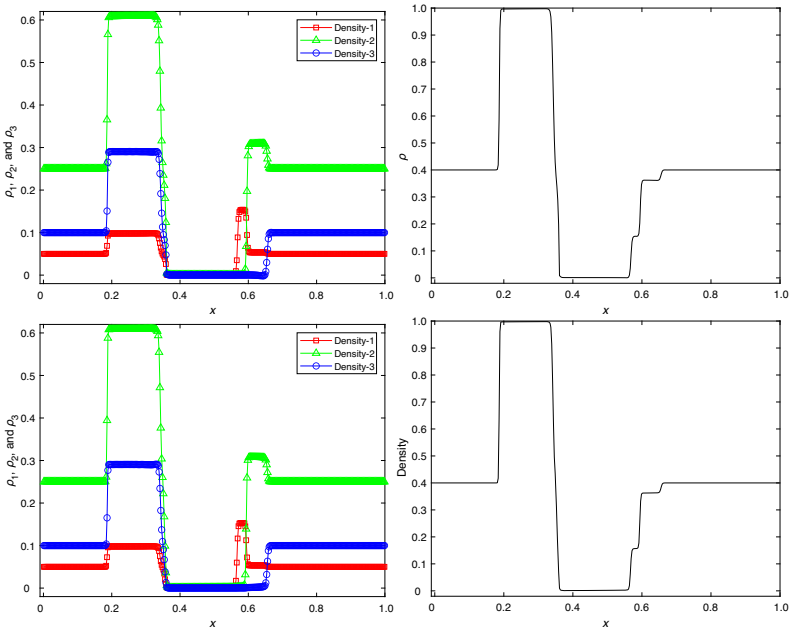

Fig. 5 ρ_1, ρ_2, ρ_3, and ρ, at $t = 30$ s. Top: solved by the hybrid WENO scheme; bottom: solved by the hybrid HWENO scheme

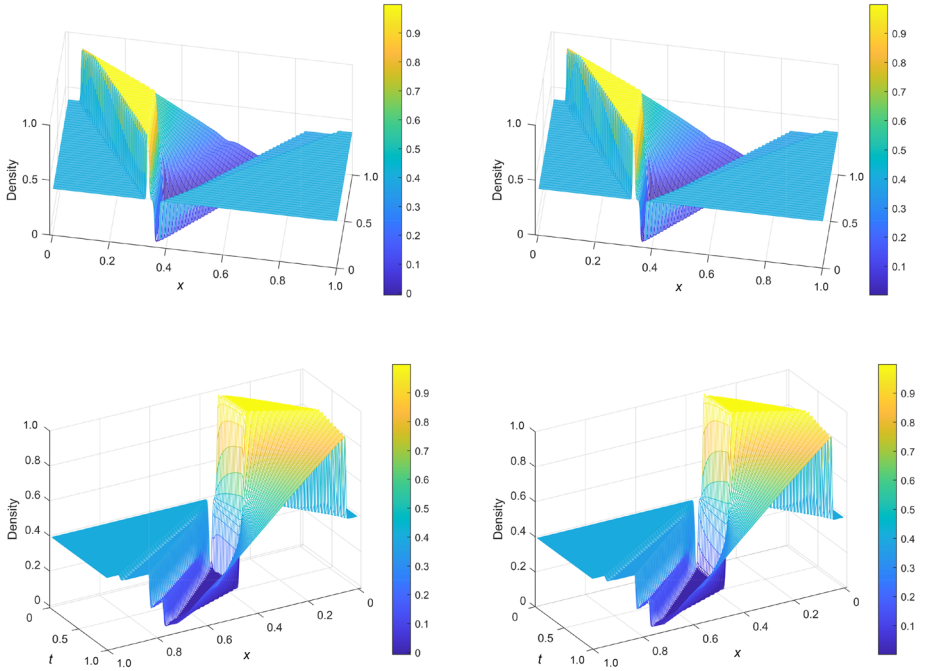

Fig. 6 Total density variation over 60 seconds. Top left: solved by the hybrid WENO scheme; top right: solved by the hybrid HWENO scheme. The bottom two images are the opposite views of the corresponding images above

5 Conclusion

In this paper, we combine the hybrid HWENO method with the TVD Runge-Kutta time discretization and apply it to the mcLWR model under inhomogeneous road conditions. Numerical examples verify the resolution and accuracy of the hybrid HWENO method. In the modified system (though non-strictly hyperbolic), the Lax-Friedrichs numerical flux provides appropriate numerical viscosity, ensuring convergence of the numerical solution to the physically relevant one. The HWENO reconstruction using the KXRCF cell indicator reduces excess numerical viscosity, achieving high-resolution solutions. The hybrid HWENO scheme's application can be used to solve other hyperbolic conservation laws that fluxes vary with space.

Funding The research is supported partly by the National Natural Science Foundation of China (Grant No. 12071392).

Declarations

Conflict of Interest On behalf of all authors, the corresponding author states that there is no conflict of interest.

References

1. Baiti, P., Jenssen, H.K.: Well-posedness for a class of 2×2 conservation laws with L^{∞} data. J. Differential Equations **140**(1), 161–185 (1997)

2. Bürger, R., Gracía, A., Karlsen, K.H., Towers, J.D.: A family of numerical schemes for kinematic flows with discontinuous flux. J. Eng. Math. **60**, 387–425 (2008)
3. Cai, X., Zhang, X., Qiu, J.: Positivity-preserving high order finite volume HWENO schemes for compressible Euler equations. J. Sci. Comput. **68**, 464–483 (2016)
4. Capdeville, G.: A Hermite upwind WENO scheme for solving hyperbolic conservation laws. J. Comput. Phys. **227**(4), 2430–2454 (2008)
5. Daganzo, C.F.: A behavioral theory of multi-lane traffic flow. Part I: long homogeneous freeway sections. Transportation Research Part B: Methodological **36**(2), 131–158 (2002)
6. Daganzo, C.F.: A behavioral theory of multi-lane traffic flow. Part II: merges and the onset of congestion. Transportation Research Part B: Methodological **36**(2), 159–169 (2002)
7. Godunov, S.: A difference scheme for numerical computation of discontinuous solution of equations of fluid dynamics. Mathematics of the USSR-Sbornik **47**, 271–306 (1959)
8. Greenshields, B.D.: An analysis of traffic flow. Proceedings of the Highway Research Board **14**, 448–477 (1934)
9. Jiang, G.-S., Shu, C.-W.: Efficient implementation of weighted ENO schemes. J. Comput. Phys. **126**(1), 202–228 (1996)
10. Klausen, R.A.: Stability of conservation laws with discontinuous coefficients. J. Differential Equations **157**(1), 41–60 (1999)
11. Krivodonova, L., Xin, J., Remacle, J.-F., Chevaugeon, N., Flaherty, J.E.: Shock detection and limiting with discontinuous Galerkin methods for hyperbolic conservation laws. Appl. Numer. Math. **48**(3/4), 323–338 (2004)
12. Lebacque, J.P.: The Godunov scheme and what it means for first order traffic flow models. In: Lesort, J.B. (ed) Proceedings of the 13th International Symposium on Transportation and Traffic Theory, pp. 647–677. Elsevier Science Ltd., Lyon, France (1996)
13. Lighthill, M.J., Whitham, G.B.: On kinematic waves II. A theory of traffic flow on long crowded roads. Proceedings of the Royal Society of London. Series A, Mathematical and Physical Sciences **229**, 317–345 (1955)
14. Lin, L., Temple, J.B., Wang, J.: Suppression of oscillations in Godunov's method for a resonant non-strictly hyperbolic system. SIAM J. Numer. Anal. **32**(3), 841–864 (1995)
15. Liu, H., Qiu, J.: Finite difference Hermite WENO schemes for hyperbolic conservation laws. J. Sci. Comput. **63**(2), 548–572 (2015)
16. Liu, H., Qiu, J.: Finite difference Hermite WENO schemes for conservation laws, II: an alternative approach. J. Sci. Comput. **66**(2), 598–624 (2016)
17. Qiu, J., Shu, C.-W.: Hermite WENO schemes and their application as limiters for Runge-Kutta discontinuous Galerkin method: one-dimensional case. J. Comput. Phys. **193**(1), 115–135 (2004)
18. Qiu, J., Shu, C.-W.: Hermite WENO schemes and their application as limiters for Runge-Kutta discontinuous Galerkin method II: two dimensional case. Computers & Fluids **34**(6), 642–663 (2005)
19. Qiu, J., Shu, C.-W.: A comparison of trouble cell indicators for Runge-Kutta discontinuous Galerkin method using WENO limiters. SIAM J. Sci. Comput. **27**, 995–1013 (2005)
20. Richards, P.I.: Shock waves on the highway. Oper. Res. **4**(1), 42–51 (1956)
21. Shu, C.-W., Osher, S.: Efficient implementation of essentially non-oscillatory shock-capturing schemes. J. Comput. Phys. **77**(2), 439–471 (1989)
22. Sun, T., Qiu, J.: LWDG method for a multi-class traffic flow model on an inhomogeneous highway. Advance in Applied Mathematics and Mechanics **1**(3), 438–450 (2009)
23. Tao, Z., Li, F., Qiu, J.: High-order central Hermite WENO schemes on staggered meshes for hyperbolic conservation laws. J. Comput. Phys. **281**, 148–176 (2015)
24. Tao, Z., Li, F., Qiu, J.: High-order central Hermite WENO schemes: dimension-by-dimension moment-based reconstructions. J. Comput. Phys. **318**, 222–251 (2016)
25. Wong, G.C.K., Wong, S.C.: A multi-class traffic flow model an extension of LWR model with heterogeneous drivers. Transportation Research Part A: Policy and Practice **36**(9), 827–841 (2002)
26. Wong, S.C., Wong, G.C.K.: An analytical shock-fitting algorithm for LWR kinematic wave model embedded with linear speed-density relationship. Transportation Research Part B: Methodological **36**(8), 683–706 (2002)
27. Wong, S.C., Wong, G.C.K.: An analytical shock-fitting algorithm for LWR kinematic wave model embedded with linear speed-density relationship. Transp. Res. **36B**, 683–706 (2002)
28. Zhang, P., Liu, R.X.: Hyperbolic conservation laws with space-dependent fluxes: II. General study of numerical fluxes. Journal of Computational and Applied Mathematics **176**(1), 105–129 (2005)
29. Zhang, P., Liu, R.X., Wong, S.C., Dai, S.Q.: Hyperbolicity and kinematic waves of a class of multi-population partial differential equations. Eur. J. Appl. Math. **17**(2), 171–200 (2006)

30. Zhang, P., Wong, S.C., Shu, C.-W.: A weighted essentially non-oscillatory numerical scheme for a multi-class traffic flow model on an inhomogeneous highway. J. Comput. Phys. **212**(2), 739–756 (2006)
31. Zhao, Z., Chen, Y., Qiu, J.: A hybrid Hermite WENO scheme for hyperbolic conservation laws. J. Comput. Phys. **405**, 109175 (2020)
32. Zhao, Z., Zhu, J., Chen, Y., Qiu, J.: A new hybrid WENO scheme for hyperbolic conservation laws. Computers & Fluids **179**, 422–436 (2019)
33. Zhu, J., Qiu, J.: A class of the fourth order finite volume Hermite weighted essentially non-oscillatory schemes. Sci. China Ser. A Math. **51**(8), 1549–1560 (2008)